

# Electronic and ionic relaxations in strontium-borate glass and glass-ceramics containing bismuth and vanadium oxides

N. A. Szreder <sup>a,\*</sup>, P. Kupracz <sup>a</sup>, M. Przeźniak-Welenc <sup>a</sup>, J. Karczewski <sup>a</sup>, M. Gazda <sup>a</sup>,  
K. Siuzdak <sup>b</sup>, R. J. Barczyński <sup>a</sup>

<sup>a</sup> Faculty of Applied Physics and Mathematics, Gdańsk University of Technology, Ul. Narutowicza 11/12, 80-233 Gdańsk, Poland

<sup>b</sup> Polish Academy of Sciences, The Szewalski Institute of Fluid-Flow Machinery, Fiszerza 14, 80-233 Gdańsk, Poland

\*corresponding author: [nszreder@mif.pg.gda.pl](mailto:nszreder@mif.pg.gda.pl)

---

## Abstract

The topography, microstructure and electrical properties of strontium-borate glass and SBO glass containing bismuth and vanadium oxides, were studied. The structure was measured using X-ray diffraction (XRD), Energy Dispersive X-ray Spectrometer (EDS) and Scanning electron microscope (SEM) methods. The A.C. complex conductivity was investigated as a function of temperature and frequency. The influence of the quantity of bismuth and vanadium oxides present, on glasses microstructure and electrical properties, was discussed.

In order to obtain glass-ceramics, the glasses were subjected to crystallization at temperatures close to the exothermic processes indicated by the differential scanning calorimetry (DSC) measurements. X-ray diffraction (XRD) measurements were carried out to determine the presence of bismuth vanadate ( $\text{Bi}_2\text{VO}_{5.5}$ ) crystalline phase in heat-treated samples. After heat-treatment, there were still some traces of the glassy phase within the samples. The effect of the crystallization process on the microstructure, topography and dielectric behavior of the material was analyzed. The A.C. dielectric permittivity, conductivity and impedance were discussed at specific temperature and frequency region, in addition conduction mechanisms were proposed.

*Keywords:* Strontium-borate glass; bismuth vanadate ceramic; impedance analysis; glass-ceramic; Cole-Cole relation.

---

## 1. Introduction

Borate glasses are known for their high thermal stability, low melting point and good solubility of rare earth ions [1]. Boron in boron-oxygen structural units has the ability to change coordination number, that is a variety of B-O structural units may be present in the glass network [2,3]. The structure of glassy  $\text{B}_2\text{O}_3$  consists of a random network of boroxol rings and  $\text{BO}_3$  triangles connected by B–O–B linkages [4]. However, this glass easily

becomes unstable due to its hygroscopic nature. Therefore in order to obtain a stable borate glass, modifiers such as alkalis and alkaline earth ions are added [5, 6]. Metal oxides like MgO, CaO, SrO, BaO, ZnO and Al<sub>2</sub>O<sub>3</sub> etc., are found to be stabilizers of borate glasses [4]. Apart from being stabilizers these oxides also modify other physical properties of the glasses. For instance strontium-borate glass SrB<sub>4</sub>O<sub>7</sub> (SBO) has dielectric, thermal and non-linear optical properties. It has a relatively low melting point and can be easily prepared by the traditional melting method. SBO glass is known as a good host matrix for easily dispersing a large number of ferroelectric crystallites [7].

Recently, borate glasses containing heavy metal oxides such as Bi<sub>2</sub>O<sub>3</sub>, PbO and Ga<sub>2</sub>O<sub>3</sub> have been also studied because of a wide number of promising applications in optical and electronic devices [8,9]. Bismuth oxide is a glass modifier which causes an increase in the density, linear and non-linear refractive indices of glass. These properties enhance their applications in optical and optoelectronics [10, 11]. Borate glasses containing Bi<sub>2</sub>O<sub>3</sub> show improved chemical durability, thermal stability and reduce the phonon energy of the glasses [12].

Vanadium oxide is a transition metal oxide which within the structure of a glass may act as both a glass former and glass network modifier. Glasses containing a large amount of transition metal oxides exhibit electronic conductivity. Their electrical properties are determined by the presence of transition metal ions in two different valence states (for instance V<sup>4+</sup> and V<sup>5+</sup>). The conductivity of these systems is usually described by the mechanism of polaron hopping between such ions [13-16]. A general formula for the electrical conductivity of these glasses was proposed by Mott in which the conductivity,  $\sigma$ , is given by [16]:

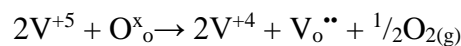
$$\sigma = \frac{v_{ph} e^2 C(1-C)}{kTR} \exp(-2\alpha R) \exp\left(-\frac{W}{kT}\right) \quad (1)$$

where  $v_{ph}$  is the phonon frequency,  $\alpha$  is the rate of wave function decay,  $C$  is the ratio of ion concentration in the low valence state to the total concentration of transition-metal ions,  $R$  is the average hopping distance,  $W$  is the activation energy,  $e$  is the electron charge,  $k$  is Boltzmann's constant and  $T$  is the absolute temperature.

There are a large number scientific papers which describe glasses containing significance quantities of V<sub>2</sub>O<sub>5</sub> (>50 % mol) for instance: V<sub>2</sub>O<sub>5</sub>-P<sub>2</sub>O<sub>5</sub> [17], Fe<sub>2</sub>O<sub>3</sub>-V<sub>2</sub>O<sub>5</sub>-P<sub>2</sub>O<sub>5</sub> [18], V<sub>2</sub>O<sub>5</sub>-Bi<sub>2</sub>O<sub>3</sub> [19], ZnO-V<sub>2</sub>O<sub>5</sub>-P<sub>2</sub>O<sub>5</sub>, GeO<sub>2</sub>-V<sub>2</sub>O<sub>5</sub>-P<sub>2</sub>O<sub>5</sub> [20] and V<sub>2</sub>O<sub>5</sub>-TeO<sub>2</sub> glasses

[21]. When comparing the electrical properties of vanadium oxide glasses, one may notice that vanadium-bismuth oxide glasses exhibit higher D.C. conductivity than those of the corresponding  $V_2O_5-P_2O_5$  and  $V_2O_5-TeO_2$  glasses [19].

The bismuth vanadate  $Bi_2VO_{5.5}$  ceramics (BiV) have ferroelectric properties at room temperature which show promise across a range of potential applications. Bismuth vanadate crystallizes in a polar orthorhombic form. It exhibits three main polymorphs which are stable at different temperature ranges. A non-centrosymmetric  $\alpha$ -phase which is stable below 730K, a centrosymmetric  $\beta$ -phase between 730K and 835K and a centrosymmetric  $\gamma$ -phase which is stable above 835K. BiV melts at 1153K. The high temperature  $\gamma$ -phase consists of  $(Bi_2O_2)^{2+}$  sheets interleaved with perovskite like layers of  $(VO_{3.5\Box_{0.5}})^{2-}$  where  $\Box$  denotes oxygen ion vacancies [22-24]. In BiV systems, oxygen vacancies could be caused by the presence of reduced valance state of vanadium ions ( $V^{4+}$ ). One oxygen ion vacancy will form with two tetravalent vanadium ions entering into the crystal structure, in order to maintain the electrical neutrality. This reaction could be described using Kroger–Vink notation:



where  $V_o^{**}$  is the oxygen vacancy with two effective positive charges and  $O^{x_o}$  is the oxygen ion in the oxygen site with zero effective charge [25]. The BiV  $\gamma$ -phase exhibits a high ionic conductivity which may be attributed to the presence of doubly charged oxygen ion vacancies  $V_o^{**}$  in the perovskite layer, considered to be the most mobile charges in perovskite ferroelectrics. The oxygen vacancies in  $\alpha$  and  $\beta$ -phases of BiV also give rise to non-negligible ionic conductivity of the order of  $10^{-6}$  to  $10^{-3} \Omega^{-1}cm^{-1}$  [22-24]. In oxygen ion conductors, current flow occurs through the movement of oxygen ions or vacancies through the crystal lattice. This movement is a result of thermally-activated hopping of the oxygen ions, moving from crystal lattice site to crystal lattice site, with a superimposed drift in the direction of the electric field. The ionic conductivity is consequently strongly temperature dependent and is also closely related to the disorder of oxygen vacancies. The number of oxides needed to consider ion oxygen conduction is relatively low and the energy involved in the process of migration from one site to the unoccupied equivalent site must be small, certainly less than about 1 eV [26].

Ferroelectric glass–ceramics have shown great potential in certain electronic applications such as thermal switches, capacitors, electrooptic devices, piezoelectric sonar and

ultrasonic transducers, radio communication filters, pyroelectric security surveillance devices, tweeters, buzzers, sensors and ferroelectric thin film memory [27-32]. Their dielectric permittivity is very sensitive to changes in grain size and to the structure of agglomerates and grain boundaries [27-32]. The most common method for obtaining such materials is using a conventional glass melting technique followed by a controlled crystallization of the glasses obtained [27]. Numerous studies of glass-ceramic composites prepared from two or more components include materials containing ferroelectric titanate and niobate crystallites such as:  $\text{LiNbO}_3$ ,  $\text{NaNbO}_3$ ,  $\text{LiTaO}_3$ ,  $\text{PbTiO}_3$ ,  $\text{BaTiO}_3$ , dispersed within an amorphous matrix formed by glass forming oxides ( $\text{SiO}_2$ ,  $\text{V}_2\text{O}_5$ ,  $\text{B}_2\text{O}_3$ ,  $\text{PbO}$ ) [27-32].

There are only a few literature reports regarding the properties of strontium-borate glasses, bismuth and vanadium oxides containing strontium-borate glasses and glass-ceramics [7, 33, 34]. Moreover, there is a lack of complex analysis of the electrical behavior of these systems. The aim of the present study is to investigate the electrical properties, morphology and structure of strontium-borate glass and strontium-borate glass containing bismuth and vanadium oxides. Moreover, the influence of the crystallization process on their structure and electrical behavior was studied.

## 2. Experimental

The polycrystalline strontium borate,  $\text{SrB}_4\text{O}_7$  was synthesized via a solid state reaction route that involved heating stoichiometric mixtures of analytical grade  $\text{SrCO}_3$  and  $\text{H}_3\text{BO}_3$  at 1073K for 12 hours. Next, samples of a composition of  $x(2\text{Bi}_2\text{O}_3-\text{V}_2\text{O}_5)-(100-x)\text{SrB}_4\text{O}_7$ , where  $x=5$  and 50 (in %mol) were prepared from reagent-grade  $\text{Bi}_2\text{O}_3$ ,  $\text{V}_2\text{O}_5$  and pre-prepared  $\text{SrB}_4\text{O}_7$ . While SBO glass samples ( $x=0$ ) were prepared from reagent-grade  $\text{SrCO}_3$  and  $\text{H}_3\text{BO}_3$ . Samples of glass were prepared by the conventional melt quenching technique. The melting was conducted in alumina crucibles at 1373 K for 2 hours. The melt was poured onto a preheated (573 K) brass plate and pressed by another plate to obtain flat circular disks of 1 - 2 mm thickness and 20 - 30 mm in diameter.

Differential scanning calorimetry (DSC) measurements were performed on powdered samples in a flow of nitrogen at  $50 \text{ cm}^3\text{min}^{-1}$  using a Netzsch STA 449F1 thermal analyzer . The heating rate was maintained at  $15 \text{ Kmin}^{-1}$  within a temperature range of 373–813 K. The presence of crystalline phases and their phase composition were studied using an X-ray diffraction (XRD) method using a Philips X'Pert Pro MPD system with  $\text{CuK}\alpha$  radiation. The XRD measurements were conducted at room temperature.



The Raman spectra were recorded by using a confocal micro-Raman spectrometer (InVia, Renishaw) with sample excitation by means of an argon ion laser emitting at 514 nm and operating at a power level of 50mW. They were excited in the range between 100 and 1200  $\text{cm}^{-1}$  five times for every sample.

The topography of the samples was investigated using a Scanning Electron Microscope (SEM), FEI Company Quanta FEG250 with Energy Dispersive X-ray Spectrometer (EDS) QUANTA. SEM measurements were conducted on samples which had been fractured and then given a 7nm gold coating, using a 30kV beam accelerating voltage with a SE-ETD detector (secondary electron - Everhart-Thornley detector) working in the high vacuum mode (pressure  $10^{-4}$  Pa).

For electrical measurements gold electrodes were evaporated onto the surface of the polished samples. Impedance measurements were carried out in a frequency range from 10 mHz to 1 MHz with an A.C. voltage of 1  $V_{\text{rms}}$  in a temperature range from 373 to 813 K with a step of 10 K using a Novocontrol Concept 40 broadband dielectric spectrometer and high temperature Novotherm HT 1600 at atmosphere pressure. A single measurement was carried out both while increasing and decreasing the temperature and in total this process lasted for about three days. Each data point was saved when the temperature achieved did not deviate from the set temperature by more than 0.5 K and was stable for 60 sec.

Two types of samples were studied: as-quenched and heat treated ( $\text{SrB}_4\text{O}_7$ ,  $5(2\text{Bi}_2\text{O}_3-\text{V}_2\text{O}_5)-95\text{SrB}_4\text{O}_7$ ,  $50(2\text{Bi}_2\text{O}_3-\text{V}_2\text{O}_5)-50\text{SrB}_4\text{O}_7$ ). Sample names were simplified to SBO, as-quenched and heat treated 5BiV-95SBO, as-quenched, partially crystallized and fully crystallized 50BiV-50SBO. Heat treated 5BiV-95SBO samples were obtained after a full cycle of high temperature electrical measurements. Partially crystallized 50BiV-50SBO samples were obtained by heat treating in air at a temperature of 693 K for three hours and then kept the samples in the furnace to cool to room temperature. The crystallization temperature was determined on the basis of the DSC spectrum. During high temperature electrical measurements of partially crystallized 50BiV-50SBO samples, further crystallization process took place. Samples after this process were described as fully crystallized.

### 3. Results

#### 3.1. Structure and morphology

Figure 1 shows the DSC spectrum for the as-quenched 50BiV-50SBO sample. This sample exhibits one exothermic process and two endothermic processes. Glass and phase transitions identified by DSC for all the samples studied are listed in table 1 together with reference values for BiV [36]. It may be seen that SBO glass exhibits the highest glass transition temperature of 887K. SBO glass containing 5 and 50% of bismuth and vanadium oxides showed a  $T_g$  of approximately 20 K and 260 K respectively lower than for SBO glass. Exothermic and endothermic processes present in the as-quenched 50BiV-50SBO sample are absent in the other samples.

Figure 2 shows XRD patterns for all the as-quenched and heat treated samples. The results for all as-quenched samples displayed a bump characteristic for amorphous materials. The SBO and 5BiV-95SBO glasses after heat treatment did not show any development of XRD reflections. The XRD pattern for the partially crystallized 50BiV-50SBO sample consisted of an amorphous halo and small reflections of the  $\text{Bi}_2\text{VO}_{5.5}$  crystalline phase. The intensity of the reflections was higher and their positions are slightly shifted towards higher angles within the pattern for the fully crystallized sample.

The Raman spectra of the as-quenched, heat-treated 5BiV-95SBO and partially crystallized 50BiV-50SBO samples are shown in Fig. 3. The as-quenched 5BiV-95SBO sample did not show any band. The Raman spectrum of this sample after heat treatment contained three broad bands with the centres at  $\sim 155$ , 772 and  $861 \text{ cm}^{-1}$ . The intensity of these bands increased and their maxima shifted to  $\sim 148$ , 692 and  $864 \text{ cm}^{-1}$  in the partially crystallized 50BiV-50SBO sample.

Figure 4 displays SEM images of fractured as-quenched samples. It can be seen that all the glass materials, exhibit a specific nanostructure. An addition of bismuth and vanadium oxides to the strontium-borate glass causes an increase in the size of the visible nanostructures. An increase of the quantity of bismuth and vanadium oxides from 5 to 50 %mol, changed the nanostructures size from a few nanometers (Fig. 4b) to hundreds of nanometers (Fig. 4c). EDS results confirmed the percentage composition of all known elements (bismuth, vanadium, strontium and boron) in the samples but small traces of aluminium were also detected. The origin of these impurities may be from alumina crucibles used.

Figure 5 shows SEM images for the fractures of heat treated samples for 5BiV-95SBO (Fig. 5a) and fully crystallized 50BiV-50SBO (Fig. 5b). The topography of the fracture surface of the heat treated 5BiV-95SBO sample was different from the as-quenched one. It

contains few bigger nanostructures and many smaller ones. The topography of the fracture surface of the partially and fully crystallized 50BiV-50SBO samples were not significantly different from the as-quenched one.

### 3.2. Electrical properties

Figure 6 presents the real part of A.C. conductivity versus temperature, at a frequency of 100 Hz (the middle point of our measurement frequency range) for SBO and 5BiV-95SBO (Fig. 6a) and for as-quenched, partially crystallized and fully crystallized 50BiV-50SBO samples (Fig. 6b). The behavior of SBO glass conductivity (open squares in Fig. 6a) was the same during the first heating-cooling cycle as well as through the next measurement. The temperature dependence of conductivity of the sample containing 5 %mol of bismuth and vanadium oxides (filled circles) was similar to that of the strontium-borate glass up to about 630 K. Above this temperature the conductivity of the 5BiV-95SBO sample was lower than SBO glass. Moreover, conductivity curves during heating and cooling did not overlap. After a full heating-cooling cycle, the conductivity of the 5BiV-95SBO sample at 373 K was of about one order of magnitude smaller than before and during the next measurement (heating and cooling) did not exhibit further evolution. The as-quenched sample containing 50 %mol of bismuth and vanadium oxides (open triangles in Fig. 6b) had a higher conductivity in comparison to the SBO glass. During the first heating the conductivity of the as-quenched 50BiV-50SBO below  $T_g$  showed a maximum which can not be explained. Within the high temperature range (above 473 K), this material showed higher conductivity during the first heating than during the first cooling. In the partially crystallized 50BiV-50SBO sample, the conductivity during the first heating (filled upside-down triangles in Fig. 6b) exhibited a significantly different trend than that of the as-quenched one. Above 693 K (the crystallization temperature) the glass-ceramic showed changes which were due to further crystallization. After completing the first thermal cycle this sample may be considered as “fully crystallized”. However this sample still contained some amorphous phase and “fully crystallized” was only used as a reference name. At the studied temperature range the as-quenched, partially crystallized and fully crystallized 50BiV-50SBO samples exhibited conductivity higher than SBO and 5BiV-95SBO glasses.

Figure 7 shows the temperature dependence of the real part of the dielectric permittivity at 100 Hz for SBO and 5BiV-95SBO (Fig. 7a) and for the as-quenched, partially crystallized and fully crystallized 50BiV-50SBO samples (Fig. 7b). It can be seen from figure



6a that SBO glass (empty squares) exhibits a rather high value of permittivity (about 14) which increases above 700K to about 15. The 5BiV-95SBO sample (filled circles in Fig. 7a) shows significantly lower permittivity than SBO glass. Below a temperature of about 630 K, the permittivity is about 8 and during the first heating above 630K it decreases to about 5. The as-quenched 50BiV-50SBO sample (empty triangles in Fig. 7b) exhibited a lower value of permittivity than the SBO glass (about 10.5). During the first heating the permittivity of this sample increased with temperature to about 20 and above 783 K it rapidly decreased to about 9. The partially crystallized 50BiV-50SBO sample (filled upside-down triangles in Fig. 7b) showed a permittivity of about 14, which is similar to that of SBO glass. This slightly increased with temperature to about 630 K and reached 15 before decreasing above 693K, reached a minimum, and above 723K started to increase again. The permittivity curve during cooling shows the behavior of the fully crystallized 50BiV-50SBO sample. It rapidly decreased as the temperature decreased to about 9.5 at 723 K. Between 723 and 350 K the permittivity slowly decreased from 9.5 to 8.5.

## 4. Discussion

### 4.1. Structure and morphology

A small amount of  $\text{Bi}_2\text{O}_3$  ( $\leq 10$  %mol) in oxide glasses acts as a network modifier and increases the degree of disorder of the host matrix. Quantities of  $\text{Bi}_2\text{O}_3$  greater than 10 %mol act as a network former and replace matrix elements [35].  $\text{V}_2\text{O}_5$  may also play a role as both a glass former and glass network modifier. This explains why the glass transition temperature (Tab. 1) decreased as a result of the addition of even a small amount of bismuth and vanadium oxides. Both the XRD and thermal analysis results indicated that there was a significant difference between the samples containing a large amount of bismuth and vanadium oxides ( $50(2\text{Bi}_2\text{O}_3-\text{V}_2\text{O}_5)-50\text{SrB}_4\text{O}_7$ ) and those either without or with only a small amount of these oxides ( $\text{SrB}_4\text{O}_7$  and  $5(2\text{Bi}_2\text{O}_3-\text{V}_2\text{O}_5)-95\text{SrB}_4\text{O}_7$ ). The obtained XRD and DSC results for samples containing 5% of bismuth and vanadium oxides did not reveal crystallization of  $\text{Bi}_2\text{VO}_{5.5}$ , but it should be taken into consideration that the methods mentioned above have limited sensitivity. The Raman spectra of heat-treated 5BiV-95SBO showed a broad band at  $\sim 861\text{ cm}^{-1}$  which was the strongest Raman band observed in the  $\text{Bi}_2\text{VO}_{5.5}$   $\alpha$ -phase [36]. Sadequa J. Patwe et al. in their work [36] defined this band with two peaks at 830 and 862  $\text{cm}^{-1}$  and assigned them to the vibration of the respectively longer and shorter V-O bonds. They also observed in the  $\text{Bi}_2\text{VO}_{5.5}$  Raman spectrum, two bands at 653 and 756  $\text{cm}^{-1}$  related



to doubly coordinated (V-O-V) oxygen atoms [36]. We also obtained in our partially crystallized 50BiV-50SBO sample the strongest Raman band at  $\sim 864\text{ cm}^{-1}$  where the XRD method confirmed the presence of the  $\text{Bi}_2\text{VO}_{5.5}$  crystalline phase. The second band observed in both heat-treated samples at  $\sim 692\text{-}772\text{ cm}^{-1}$  was broad and we suppose that it may consist of two or more bands and may be related to doubly coordinated (V-O-V) oxygen atoms.

Additionally, some indications were observed that the 5BiV-95SBO sample undergoes structural changes as a result of heating these were provided by the SEM micrographs directly (Fig. 5a) and indirectly by results of electrical measurements. For instance, the real part of the conductivity and dielectric permittivity of 5BiV-95SBO (filled circles in Fig. 6a and 7a) exhibited pronounced changes only during the first heating. The real part of both conductivity and dielectric permittivity decreased as a result of heating in a similar way as for the 50BiV-50SBO sample (Fig. 6b and 7b). The origin of these changes is similar in both materials. Therefore, we believe that the crystallization process also occurs in 5BiV-95SBO but the size and quantity of nanocrystallites created may be too low to be detected using the DSC and XRD methods.

The as-quenched 50BiV-50SBO sample was the only sample in which the exothermic process above 683 K was detected (Fig. 1). It may be interpreted that this is as a result of the crystallization process of the  $\text{Bi}_2\text{VO}_{5.5}$  phase. This is supported by the XRD results (Fig. 2) which confirmed that the partially and fully crystallized 50BiV-50SBO samples contained the  $\text{Bi}_2\text{VO}_{5.5}$  phase. The size of the nanocrystallites obtained was calculated from the XRD spectrum of the fully crystallized sample with the use of Scheerer's formula. They had a mean size of about 30 (+/-) 3 nm. The amorphous halo slightly affected the calculations and influenced their precision. Because of the presence of  $\text{Bi}_2\text{VO}_{5.5}$  in the 50BiV-50SBO samples, other processes known to be present in this ferroelectric oxide should have been observed. In particular, at 715 K the  $\alpha \leftrightarrow \beta$  phase change occurs whereas at 841 K the  $\beta \leftrightarrow \gamma$  endothermic phase transition in  $\text{Bi}_2\text{VO}_{5.5}$  could be expected [37]. The  $\alpha \leftrightarrow \beta$  phase transition was not visible in our sample (Tab. 1), because the temperature of the exothermic process corresponding to the  $\text{Bi}_2\text{VO}_{5.5}$  crystallization is close to the temperature of the  $\alpha \leftrightarrow \beta$  endothermic phase transition and so this may mask this transition process. The  $\beta \leftrightarrow \gamma$  phase transition can be seen as the endothermic process at 838 K, very close to 841 K which is the  $\beta \leftrightarrow \gamma$  phase transition temperature in the  $\text{Bi}_2\text{VO}_{5.5}$  ceramics [37]. The endothermic process at 899 K is caused by the start of the melting process.

#### 4.2. A.C. response - temperature dependence of permittivity

The real part of the dielectric permittivity of all samples, even for the SBO glass, is rather high. The crystallization process of samples with bismuth and vanadium oxides causes a decrease of dielectric permittivity. All 50BiV-50SBO samples after crystallization exhibited an increase in permittivity with increasing temperature starting at a temperature of 725K. This increase may be attributed to the para-ferroelectric phase transition characteristic for the  $\text{Bi}_2\text{VO}_{5.5}$  crystalline phase. It could be expected that the real part of the dielectric permittivity of the materials containing a significant amount of the ferroelectric  $\text{Bi}_2\text{VO}_{5.5}$  phase is much higher (of an order of  $10^4$  or even greater) than observed in our samples. However ferroelectric BiV ceramics do not show a peak typical for ferroelectrics in dielectric permittivity due to the para-ferroelectric phase transition [38]. The dielectric permittivity of these materials increases even above the Curie temperature as has been also observed in our samples. These increases in the high temperature region may be explained by charge accumulation at the grain boundaries and electrodes which is often observed in ionic conductors.

Other reports regarding the dielectric properties of samples similar to our own showed various results [7, 33, 34]. For instance, Varma et al. [34] measured the dielectric properties of  $x\text{Bi}_2\text{VO}_{5.5}-(100-x)\text{SrB}_4\text{O}_7$  glass and glass-ceramic materials prepared from pre-prepared  $\text{Bi}_2\text{VO}_{5.5}$  and  $\text{SrB}_4\text{O}_7$  across a narrow frequency range. They observed anomalies around the Curie temperature of  $\text{Bi}_2\text{VO}_{5.5}$  and values of dielectric permittivity similar to our own (between 9 and 15). For  $50\text{Bi}_2\text{VO}_{5.5}-50\text{SrB}_4\text{O}_7$  glass-ceramic they obtained a  $\text{Bi}_2\text{VO}_{5.5}$  crystalline phase with an average grain size of 25 nm. They suggested that individual phases of BiV and SBO glass coexist in this mixture [34]. We also believe that in our samples there existed a similar situation.

Different results were reported by Syam Prasad et al. [7] who analyzed the dielectric behavior of  $x\text{Bi}_2\text{VO}_{5.5}-(100-x)\text{SrB}_4\text{O}_7$  glass and glass-ceramics prepared from pre-reacted reagents ( $\text{SrB}_4\text{O}_7$  and  $\text{Bi}_2\text{VO}_{5.5}$ ) as in Varma et al. work [34]. They obtained very high values of dielectric permittivity for their  $50\text{Bi}_2\text{VO}_{5.5}-50\text{SrB}_4\text{O}_7$  samples (around 100000) and observed a peak in dielectric permittivity near the phase-transition temperature for BiV ferroelectric. Syam Prasad et al. explained the increase in the dielectric permittivity in the as-quenched sample with temperature by the crystallization and growth of the BiV phase dispersed within SBO glass matrix. This crystallization process increases the volume of ordered polar region within the glass matrix. In this situation they may allow good

connectivity between the BiV nanocrystallites and therefore their characteristic properties begin to dominate. They also observed a decrease in the real part of the dielectric permittivity within the high temperature range after the crystallization process as in our samples. They suggested that this behavior may be attributed to a larger surface area (smaller crystallites) in the as-quenched sample, and as a consequence, higher polarization associated with them. However they observed that heat-treated samples exhibited higher values of dielectric permittivity than as-quenched ones within the low temperature range. They suggested that this was caused by the presence of strong dipolar interactions involved in the glass [7]. We have also noticed similar behavior in our material, but only after partial crystallization. We suppose that in our partially and fully crystallized 50BiV-50SBO samples the quantity and size of the Bi<sub>2</sub>VO<sub>5.5</sub> nanocrystallites produced was too small to observe values of dielectric permittivity typical for ferroelectrics. Some part of the bismuth and vanadium oxides still play a role of glass former and built the glass matrix even after crystallization process.

#### 4.3. A.C. response - Cole Cole analysis

Various processes of conductivity are visible within different frequency and temperature regions, therefore impedance spectroscopy measurements across a wide frequency range may provide some clues to identify and analyze the individual processes present [39, 40]. Different techniques: dielectric permittivity, conductivity and impedance may give a clearer picture within the specified temperature and frequency region.

The complex dielectric permittivity versus frequency and temperature describes the dielectric polarization processes. Modeling of these relaxation processes may be carried out using different empirical relations: Debye, Cole-Cole, Cole-Davidson and Havriliak-Negami [41]. In our samples we use the Cole-Cole model which describes the polydispersive nature of the dielectric relaxation. The complex dielectric permittivity for the Cole–Cole distribution may be written as [41]:

$$\varepsilon^* = \varepsilon_\infty + \frac{\varepsilon_s - \varepsilon_\infty}{1 + (j\omega\tau)^{1-\alpha}} \quad (2)$$

where  $\varepsilon^*$  is the dielectric permittivity,  $\varepsilon_s$  and  $\varepsilon_\infty$  are the static and high-frequency limiting dielectric permittivity,  $\tau$  is the mean dielectric relaxation time, and  $\alpha$  is a parameter lower than 1 [39, 40]. Figure 8 shows complex dielectric permittivity plots at different temperatures for as-quenched (Fig. 8a), partially (Fig. 8b) and fully crystallized (Fig. 8c)

50(2Bi<sub>2</sub>O<sub>3</sub>-V<sub>2</sub>O<sub>5</sub>)-50SrB<sub>4</sub>O<sub>7</sub> samples. Some dielectric polarization processes (one, two or three) are visible within various temperature range between 403 K and 473-543 K in all three samples. SrB<sub>4</sub>O<sub>7</sub> and 5(2Bi<sub>2</sub>O<sub>3</sub>-V<sub>2</sub>O<sub>5</sub>)-95SrB<sub>4</sub>O<sub>7</sub> glasses did not show any distinctive semicircles in Cole-Cole plots and are not presented. The relaxation processes responsible for particular semicircles may be due to a charge transport mechanism (for instance polaron or ion hopping) or a space charge polarization. A shift with temperature suggests that the dielectric polarization processes observed are thermally activated. The complex dielectric constant in the as-quenched, partially crystallized and fully crystallized 50BiV-50SBO samples were fitted using one, two or three Cole-Cole relaxations respectively. The outcome of successful experimental data fitting is shown in insets within Fig. 8. Figure 9 presents the mean relaxation time of the relaxation processes as a function of temperature for as-quenched, partially crystallized and fully crystallized 50BiV-50SBO samples. The relaxation time for thermally activated relaxation is described by the relation [42]:

$$\tau = \tau_0 \exp\left(\frac{E_A}{kT}\right) \quad (3)$$

where:  $\tau_0$  is the relaxation time at an infinite temperature and  $E_A$  is the activation energy. The as-quenched 50BiV-50SBO sample (filled squares in Fig. 9) shows one clear relaxation process which exhibits higher values of relaxation time than the observed in partially and fully crystallized samples. After partial crystallization this sample showed significantly different behavior. It shows two relaxation processes where a faster process (which occurred in the high frequency region - filled circles in Fig. 9) exhibited a higher activation energy, than the slower one (low frequency - empty circles). The further crystallization results in a change in the activation energy of these two processes and the beginnings of a third relaxation process. In partially and fully crystallized samples some part of the vanadium ions join bismuth ions and create bismuth vanadate nanocrystallites. The calculated values of the activation energy for the relaxation processes in the analyzed samples has a sensible physical value for both polaron and ion hopping processes.

We believe that one observed relaxation process in the as-quenched sample is due to a conduction process within the glass matrix. We suppose that in partially and fully crystallized sample two processes are due to conduction processes through two regions: Bi<sub>2</sub>VO<sub>5.5</sub> nanocrystallites and the glass matrix surrounding the nanocrystallites. We believe that the third process, whose development is observed only in the fully crystallized sample is due to the effect of nanocrystallites boundaries.



Syam Prasad et al. [7] in their work also calculated the activation energy of dielectric relaxation, observed in frequency dependence of dielectric loss for as-quenched and heat treated  $50\text{Bi}_2\text{VO}_{5.5}\text{-}50\text{SrB}_4\text{O}_7$  samples. However they analyzed only one process across a narrower frequency range. They found that the activation energy increased from 0.44 eV for the as-quenched sample to 0.57 eV after heat treatment. These low values for the activation energy were attributed to the energy levels created by donor or acceptor like states in the vicinity of the conduction or valence bands [7]. The activation energy observed in our as-quenched, partially and fully crystallized  $50\text{BiV}\text{-}50\text{SBO}$  samples were significantly higher. We believe that in our samples the processes observed are due to charge transport (polaron or ion hopping) within different regions.

#### 4.4. A.C. response - frequency and temperature dependence of A.C. conductivity

The frequency dependence of A.C. conductivity in a variety of materials have been found to obey a power law proposed by Jonscher [41]:

$$\sigma'(\omega) = A(T)\omega^{s(T)} + \sigma_{DC} \quad (4)$$

where  $\sigma'(\omega)$  is the real part of total conductivity,  $\sigma_{DC}$  is the frequency independent (D.C.) conductivity and the coefficient  $A$  and exponent  $s$  ( $0 < s < 1$ ) are dependent on temperature and material properties. The term  $A\omega^s$  contains the A.C. dependence and characterizes dispersion. However some materials, for instance ceramics, show two dispersion regions in the conductivity spectra. In these situations the A.C. conductivity follows the double power law relation [43]:

$$\sigma'(\omega) = \sigma_{DC} + A_{lf}(T)\omega^{s_{lf}(T)} + A_{hf}(T)\omega^{s_{hf}(T)} \quad (5)$$

where the exponent  $0 < s_{lf} < 1$ , characterizes the low-frequency dispersion corresponding to the translation ion hopping and the exponent  $1 < s_{hf} < 2$  characterizes the high frequency dispersion, indicating the existence of well localized relaxation process [43]. The conductivity spectra of our samples showed good agreement with the above equation at temperatures where relaxations are not observed. Figure 10 presents the real part of the conductivity as a function of frequency at several temperatures for the partially crystallized  $50\text{BiV}\text{-}50\text{SBO}$  sample. The solid lines represent the results of Eq. (5) the fit for these are in good agreement with experimental data. Similar behavior was observed for the SBO glass, heat treated  $5\text{BiV}\text{-}$

95SBO and fully crystallized 50BiV-50SBO samples. Figure 11a shows  $A_{hf}$ ,  $A_{lf}$  dispersion parameters and figure 11b presents  $s_{hf}$ ,  $s_{lf}$  parameters as a function of temperature. It may be seen that the SBO glass (empty squares) and heat treated 5BiV-95SBO sample (empty circles) show similar values for both parameters in the high-frequency dispersion. While 5BiV-95SBO glass (filled circles), partially (filled triangles) and fully crystallized (filled upside-down triangles) 50BiV-50SBO samples exhibited similar values of  $s$  and  $A$  parameters in the low-frequency dispersion. Partially (empty triangles) and fully crystallized (empty upside-down triangles) 50BiV-50SBO samples have significantly different parameters for the high-frequency dispersion from those of the SBO glass and heat treated 5BiV-95SBO sample. The further crystallization process found within the partially crystallized 50BiV-50SBO sample caused only slight changes to the  $s$  and  $A$  parameters in the both high and low-frequency dispersion areas.

#### 4.5. D.C. response - temperature dependence of conductivity

The D.C. conductivity versus the reciprocal of the temperature for the samples studied is presented in figure 12. These values were calculated from a plateau (which was found in the low frequency region) observed in the frequency dependence of the real part of the conductivity. It can be seen that the as-quenched (filled circles) and heat treated samples (empty triangles) containing 5 %mol of bismuth and vanadium oxides had the lowest D.C. conductivity. The partially crystallized 50BiV-50SBO sample (crosses) showed significantly higher D.C. conductivity than the SBO glass (empty squares). The further crystallization process of the  $\text{Bi}_2\text{VO}_{5.5}$  phase decreased the D.C. conductivity (filled triangles). Figure 12 also presents the values for the activation energy of the D.C. conduction processes for all samples occurring in the high temperature region evaluated using the Arrhenius relation:

$$\sigma_{DC} T = \sigma_0 \exp\left(\frac{E_A}{kT}\right) \quad (6)$$

where  $\sigma_{DC}$  is the D.C. conductivity,  $\sigma_0$  is a constant and  $E_A$  is the activation energy.

It can be seen that the conductivity in SBO glass exhibited almost the same activation energy as in the as-quenched 5BiV-95SBO sample in the first heating. Under cooling and for the next electrical measurement, the heat treated 5BiV-95SBO sample showed a slightly higher activation energy, which confirmed that some changes in the nanostructure took place. The value of the activation energy for SBO glass, as -quenched and heat treated 5BiV-95SBO

samples had values which were indicative of ion hopping process. We believe that in these samples the conduction mechanism was due to oxygen vacancies.

Oxide glasses containing large quantities of vanadium ions exhibit the electronic conductivity described by the mechanism of small polaron hopping [13-16]. We believe that in the as-quenched 50BiV-50SBO sample besides oxide ion hopping between vacancies, another conduction mechanism may coexist due to polaron hopping between vanadium ions in two different valence states. The crystallization process causes both a depletion of the glass matrix in vanadium ions and allows the formation of the  $\text{Bi}_2\text{VO}_{5.5}$  crystalline phase. The lower concentration of vanadium ions in the glass leads to a decrease of the glass conductivity (Fig. 6b). However some part of the bismuth and vanadium oxides even after the crystallization process, still play a role as a glass former and comprise part of the glass matrix within the SBO glassy phase. On the other hand it is known that the crystalline  $\text{Bi}_2\text{VO}_{5.5}$  phase also contains vanadium ions in two different valence states and exhibits a relatively high ionic conductivity for the high temperature  $\beta$  structure ( $0.01 \text{ Scm}^{-1}$  at 773K). Below the transition temperature (715 K) the conductivity is lower ( $10^{-5} \text{ Scm}^{-1}$  at 573K) [37]. The activation energy for the conductivity was 1 and 0.6 eV, respectively. Therefore, it may be expected that the influence of crystallization on the electrical properties of the studied materials is complex. Both partially and fully crystallized 50BiV-50SBO samples showed significantly lower D.C. conductivity and higher activation energy than  $\text{Bi}_2\text{VO}_{5.5}$  ceramics (Fig. 12). The activation energy for the D.C. conductivity of both samples was close to those for the SBO glass. This indicated that it was the glass matrix which determined the total D.C. conductivity of the material. When there are vanadium ions in two different valence states and oxygen vacancies present in both the glass matrix and  $\text{Bi}_2\text{VO}_{5.5}$  crystalline phase of partially and fully crystallized 50BiV-50SBO samples, we believe that the D.C. conduction mechanism is mixed ionic-electronic. However, the ionic mechanism begins to dominate at higher temperatures.

#### 4.6. A.C. response – the frequency and temperature dependence of complex impedance

In the high temperature region the most convenient representation of our data is the frequency dependence of the imaginary and real part of the impedance. We used the Cole-Cole expression to analyze the experimental data, which is given by [39, 40]:

$$Z^* = \frac{R}{1 + (j\omega\tau)^{1-\alpha}} \quad (7)$$





where  $Z^*$  is the complex impedance,  $R$  is resistance,  $\tau$  is the mean dielectric relaxation time and  $\alpha$  is a parameter which describes the width of the relaxation time distribution. It is known that the lower the  $\alpha$  parameter, the narrower the distribution of the relaxation time is, and the more ordered the structure is [39, 40]. Figure 13 shows an example of a Nyquist plot (real versus imaginary part of the impedance) for SBO glass (Fig. 13a), a heat treated 5BiV-95SBO sample (Fig. 13b) and a fully crystallized 50BiV-50SBO sample (Fig. 13c) at 813 K. The first two samples show two overlapping semicircles which are due to two relaxation processes and the glass-ceramic exhibits three relaxation processes (the arcs centers correspond to the identified frequency values). The solid lines in figure 13 represent the results of fitting which are in good agreement with the experimental data. At temperatures lower than 723 K the relaxation process is shifted into the low frequency region outside our range of measurement in all three samples, therefore it was not possible to fulfill the fitting. As-quenched 5BiV-95SBO and, as-quenched and partially crystallized 50BiV-50SBO samples were not analyzed because of crystallization process. The conductivities were calculated from resistances determined using relation (7). Figures 14 (a) and (b) show the temperature dependence of the following: relaxation time and conductivity for SBO (squares), heat treated 5BiV-95SBO (circles) and fully crystallized 50BiV-50SBO (triangles) samples. Figure 15 displays the  $\alpha$  parameter and table 2 presents  $\tau_0$ ,  $\sigma_0$ , activation energy calculated from figure 14 with relations (3) and (6). SBO glass showed two relaxation processes where the faster process (in the high frequency region - filled squares) is described by higher conductivity and activation energy ( $E_A(\sigma)$  and  $E_A(\tau)$ ) than the slower process (low frequency - empty squares). This process also showed a higher value of  $\sigma_0$ , lower  $\tau_0$  and slightly higher  $\alpha$  (less ordered structure). The addition of 5 %mol of bismuth and vanadium oxides to SBO glass and heat treating slightly changed all parameters. The heat treated 5BiV-95SBO sample showed higher conductivity and lower activation energy for the high frequency process (filled circles) than SBO and the opposite in the low frequency process (empty circles). However in this sample the  $\alpha$  parameter is lower for the faster process. In the fully crystallized 50BiV-50SBO sample the fastest process (filled triangles) exhibited the highest conductivity and the lowest activation energy for the conduction process. It also shows the lowest  $\alpha$  (the narrowest distribution for the relaxation time).

On the basis of parameters for all of the observed processes within the samples analyzed, it can be seen, that for the SBO glass and heat treated 5BiV-95SBO sample the high



frequency process is due to an ionic conduction process through the all glassy sample. The low frequency process is due to electrode effects which are usually visible at high temperatures and show high values of relaxation time. In the fully crystallized 50BiV-50SBO sample, the high-frequency process was due to an ionic conduction process through nanocrystallites of the  $\text{Bi}_2\text{VO}_{5.5}$  phase, the intermediate-frequency process (empty triangles) proceeded within the residual glass matrix which surrounded the nanocrystallites and the low-frequency process (crossed empty triangles) is associated with the grain boundary.

To sum up, the structure of SBO glass is homogeneous and the conduction mechanism is ionic. The 5BiV-95SBO sample contains two phases: nanostructures and the residual glass matrix. Heat treatment of this sample changes its nanostructure and electrical properties. It shows two dispersions in conductivity within the medium temperature range. The parameters of conduction within the glass matrix are similar in both SBO and heat treated 5BiV-95SBO samples. Parameters of conduction within nanostructures are similar to those observed in the BiV crystalline phase.

The electrical behavior of the as-quenched 50BiV-50SBO sample may be analyzed only within the low temperature region below the crystallization onset temperature. This sample contained two amorphous phases and the conduction mechanism in this sample may be mixed electronic-ionic. The partially crystallized 50BiV-50SBO sample was analyzed in the temperature range up to  $T_{cr}$ . This sample contained BiV nanocrystallites placed in an amorphous glass matrix. The conduction process of this material showed different parameters when it occurred within the crystalline phase and within the glass matrix. After further crystallization, (in the fully crystallized sample) the BiV nanocrystallites influenced the impedance spectra causing an additional relaxation process. We believe that after the crystallization process in the 50BiV-50SBO sample, some part of the bismuth and vanadium ions still play a role as a glass former. This may explain the change in the dielectric behavior observed with increasing temperature. Within the low temperature range the conduction mechanism is mixed electronic and ionic, however the mobility of the oxygen vacancies is lower than that of polarons. When the temperature increases, the mobility of the oxygen ions also increases and the ionic mechanism starts to be dominate. The glass matrix also contains oxygen vacancies, however within the high temperature range the conductivity of the glass matrix is lower than that of the nanocrystallites.

## 5. Conclusions

To conclude, the SBO glass, SBO glass containing bismuth and vanadium oxides and glass-ceramics were prepared. Structure investigations showed that all as-quenched samples were amorphous and consisted of nanostructures which were not visible in the XRD spectra. In the  $50(2\text{Bi}_2\text{O}_3\text{-V}_2\text{O}_5)\text{-50SrB}_4\text{O}_7$  glass, the heat treatment above 613 K resulted in the crystallization of the  $\text{Bi}_2\text{VO}_{5.5}$  phase, which was visible as ordered nanocrystallites. The crystallization process was visible due to a significant decrease in A.C. and D.C. conductivity and dielectric permittivity values, despite the fact that the  $\text{Bi}_2\text{VO}_{5.5}$  crystals are ferroelectric. No para-ferroelectric phase transition was observed in the  $50(2\text{Bi}_2\text{O}_3\text{-V}_2\text{O}_5)\text{-50SrB}_4\text{O}_7$  samples before or after the crystallization process.

In the  $\text{SrB}_4\text{O}_7$  and  $5(2\text{Bi}_2\text{O}_3\text{-V}_2\text{O}_5)\text{-95SrB}_4\text{O}_7$  samples the low frequency relaxation process was due to ionic conduction through the whole glassy sample. The as-quenched  $50(2\text{Bi}_2\text{O}_3\text{-V}_2\text{O}_5)\text{-50SrB}_4\text{O}_7$  sample consisted of two different amorphous phases and exhibited one conduction process within the glass matrix. In the partially crystallized  $50(2\text{Bi}_2\text{O}_3\text{-V}_2\text{O}_5)\text{-50SrB}_4\text{O}_7$  samples one relaxation process was due to the conduction process within the glass matrix and the second process was due to the conduction process through the crystalline phase of the  $\text{Bi}_2\text{VO}_{5.5}$ . After the further crystallization process for this sample and within the high temperature region, the conduction through the nanocrystallites started to dominate and the third relaxation process appeared which was due to the nanocrystallites boundaries. The conduction mechanism in the as-quenched, partially and fully crystallized  $50(2\text{Bi}_2\text{O}_3\text{-V}_2\text{O}_5)\text{-50SrB}_4\text{O}_7$  samples, within the low temperature region, may be due to polaron hopping between vanadium ions at two different valence states or ion hopping between oxygen vacancies. Within the high temperature region the dominating conduction mechanism in all samples studied was ionic conduction.

## References

- [1] S. Mohan, K.S. Thind, G. Sharma, *Braz. J. Phys.* 37 (2007) 1306-1313.
- [2] W.L. Konijnendijk, J.M. Stevels, in: L.D. Pye, V.D. Frechette, N.J. Kreidl (Eds.), *Borate Glass: Structure, Properties and Applications*, Plenum Press, New York, 1978, pp. 259.
- [3]: G.D. Chryssikos, E.I. Kamitsos, in: A.C. Wright, S.A. Feller, A.C. Hannon (Eds.), *Proc. 2nd Intern. Conf. Borate Glasses, Crystals and Melts*, Society of Glass Technology, Sheffield, UK, 1997, pp 128-139.
- [4] J. Krogh-Moe, *Phys. Chem. Glasses* 6 (1965) 46-54.



- [5] B. Sumalatha, I. Omkaram, T. Rajavardhana Rao, Ch. Linga Raju, *J. Non-Cryst. Solids* 357 (2011) 3143-3152.
- [6] M. Santiago, J. Marcazzó, C. Grasselli, A. Lavat, P. Molina, F. Spano, E. Caselli, *Radiat. Meas.* 46 (2011) 1488-1491.
- [7] N. Syam Prasad, K.B.R. Varma, B. Lang Sidney, *J. Phys. Chem. Solids* 62 (2001) 1299-1311.
- [8] D.W. Hall, M.A. Newhouse, N.F. Borelli, W.H. Dumbaugh, D.L. Weidman, *Appl. Phys. Lett.* 54 (1989) 1293-1295.
- [9] C. Stehle, C. Vira, D. Hogan, S. Feller, M. Affatigato, *Phys. Chem. Glasses* 39 (1998) 83-86.
- [10] E. Culea, L. Pop, P. Pascuta, M. Bosca, *J. Mol. Struct.* 924–926 (2009) 192-195.
- [11] A. Agarwal, V.P. Seth, P.S. Gahlot, S. Khasa, P. Chand, *J. Phys. Chem. Solids* 64 (2003) 2281-2288.
- [12] D. Rajesh, Y.C. Ratnakaram, M. Seshadri, A. Balakrishna, T. Satya Krishna, *J. Lumin.* 132 (2012) 841-849.
- [13] L. Murawski, C.H. Chung, J.D. Mackenzie, *J. Non-Cryst. Solids* 32 (1979) 91-104.
- [14] L. Murawski, C.H. Chung, J.D. Mackenzie, *Rev. Chim. Miner.* 16 (1979) 308-327.
- [15] L. Murawski, *J. Mater. Sci.* 17 (1982) 2155-2163.
- [16] N.F. Mott, *J. Non-Cryst. Solids* 1 (1968) 1-17.
- [17] T.K. Pietrzak, J.E. Garbarczyk, I. Gorzkowska, M. Wasiucionek, J.L. Nowinski, S. Gierlotka, P. Jozwiak, *J. Power Sources* 194 (2009) 73-80.
- [18] H. Hirashima, M. Mitsuhashi, T. Yoshida, *J. Ceram. Soc. Jpn.* 90 (1982) 411-419.
- [19] A. Gosh, B.K. Chaudhuri, *J. Non-Cryst. Solids* 83 (1986) 151-161.
- [20] H. Hirashima, H. Kurokawa, K. Mizobuchi, T. Yoshida, *Glastech. Ber.* 61 (1988) 151-156.
- [21] T. Sankarappa, M. Prashant Kumar, G.B. Devidas, N. Nagaraja, R. Ramakrishnareddy, *J. Mol. Struct.* 889 (2008) 308-315.
- [22] F. Abraham, J.C. Boivin, G. Mairesse, G. Nowogrocki, *Solid State Ionics* 40-41 (1990) 934-937.
- [23] K.B.R. Varma, G.N. Subbanna, T.N. Guru Row, C.N.R. Rao, *J. Mater. Res.* 5 (1990) 2718-2722.
- [24] K.V.R. Prasad, K.B.R. Varma, *J. Mater. Sci.* 30 (1995) 6345-6349.
- [25] Neelam Kumari, S.B. Krupanidhi, K.B.R. Varma, *Mat. Sci. Eng. B* 138 (2007) 22–30.
- [26] S.J. Skinner, J.A. Kilner, *Mater. Today* 6 (2003) 30-37.



- [27] M.S. Al-Assiri, M.M. El-Desoky, A. Al-Hajry, A. Al-Shahrani, A.M. Al-Mogeeth, A.A. Bahgat, *Physica B* 404 (2009) 1437-1445.
- [28] S. Ezhilvalavan, J.M. Xue, Wang John., *Mater. Chem. Phys.* 75 (2002) 50-55.
- [29] A.M. Glass, M.E. Lines, K. Nassau, J.W. Shiever, *Appl. Phys. Lett.* 31 (1977) 249-251.
- [30] N.V. Golubev, V.N. Sigaev, S.Yu. Stefanovich, T. Honma, T. Komatsu, *J. Non-Cryst. Solids* 354 (2008) 1909-1914.
- [31] M.P.F. Graca, M.G. F. da Silva, M.A. Valente, *J. Eur. Cer. Soc.* 28 (2008) 1197-1203.
- [32] M.E. Lines, *Phys. Rev. B* 15 (1977) 388-395.
- [33] M.V. Shankar, K.B.R. Varma, *J. Non-Cryst. Solids* 226 (1998) 145-154.
- [34] K.B.R. Varma, M.V. Shankar, G.N. Subbanna, *Mater. Res. Bull.* 31 (1996) 475-482.
- [35] M. Rada, L. Rus, S. Rada, E. Culea, T. Rusu, *Spectrochim. Acta A Mol. Biomol. Spectrosc.* 132 (2014) 533-537.
- [36] S.J. Patwe, A. Patra, R. Dey, A. Roy, R.M. Kadam, S.N. Achary, A.K. Tyagi, *J. Am. Ceram. Soc.* 96 11 (2013) 3448-3456.
- [37] G. Mairesse, P. Roussel, R.N. Vannier, M. Anne, G. Nowogrocki, *Solid State Sci.* 5 (2003) 861-869.
- [38] N.A. Szreder, P. Kupracz, M. Prześniak-Welenc, J. Karczewski, M. Gazda, R.J. Barczyński, *Solid State Ionics* 271 (2015) 86-90.
- [39] J.R. Macdonald, D.R. Franceschetti, in: J.R. Macdonald (Eds.), *Impedance Spectroscopy Emphasizing Solid Materials and Systems*, Wiley, New York, 1987, pp. 98.
- [40] E. Barsoukov, J.R. Macdonald, *Impedance Spectroscopy Theory, Experiment, and Applications*, Wiley, 2005.
- [41] A.K. Jonscher, *Dielectric Relaxation in Solids*, Chelsea Dielectrics, London, 1983.
- [42] Elliott R., *Adv. Phys.* 36 (1987) 135-218.
- [43] A.S. Nowick, B.S. Lim, A.V. Vaysleyb, *J. Non-Cryst. Solids* 172-174 (1994) 1243-1251.

### Captions

**Figure 1.** The DSC spectrum for the as-quenched  $50(2\text{Bi}_2\text{O}_3\text{-V}_2\text{O}_5)\text{-}50\text{SrB}_4\text{O}_7$  sample.

**Figure 2.** XRD spectra for as-quenched and heat-treated samples at room temperature.

**Figure 3.** FT-Raman spectra for as-quenched, heat-treated 5BiV-95SBO and partially crystallized 50BiV-50SBO samples.

**Figure 4.** SEM pictures of fractured as-quenched samples  $x(2\text{Bi}_2\text{O}_3\text{-V}_2\text{O}_5)\text{-}(100\text{-}x)\text{SrB}_4\text{O}_7$ , where  $x=0$  (a), 5 (b) and 50 (c) (in % mol).



**Figure 5.** SEM pictures of fractured heat treated samples  $x(2\text{Bi}_2\text{O}_3\text{--V}_2\text{O}_5)\text{--}(100\text{--}x)\text{SrB}_4\text{O}_7$ , where  $x=5$  (a) and 50 (b) (in % mol).

**Figure 6.** The temperature dependence of the real part of A.C. conductivity at 100Hz for (a) SBO and 5BiV-95SBO and (b) as-quenched, partially crystallized and fully crystallized 50BiV-50SBO samples.

**Figure 7.** The temperature dependence of the real part of dielectric permittivity at 100Hz for (a) SBO and 5BiV-95SBO and (b) as-quenched, partially crystallized and fully crystallized 50BiV-50SBO samples.

**Figure 8.** Cole-Cole plots for (a) as-quenched, (b) partially crystallized and (c) fully crystallized 50BiV-50SBO samples.

**Figure 9.** Temperature dependence of the mean relaxation time of dielectric loss for as-quenched, partially crystallized and fully crystallized  $50(2\text{Bi}_2\text{O}_3\text{--V}_2\text{O}_5)\text{--}50\text{SrB}_4\text{O}_7$  samples.

**Figure 10.** The real part of the conductivity as a function of frequency at several temperatures for partially crystallized  $50(2\text{Bi}_2\text{O}_3\text{--V}_2\text{O}_5)\text{--}50\text{SrB}_4\text{O}_7$  sample. The solid lines in the picture represent the results of fitting.

**Figure 11.** Temperature dependence of (a) A and (b) s dispersion parameters of double power law relation fitting for SBO, heat treated  $5(2\text{Bi}_2\text{O}_3\text{--V}_2\text{O}_5)\text{--}95\text{SrB}_4\text{O}_7$ , partially and fully crystallized  $50(2\text{Bi}_2\text{O}_3\text{--V}_2\text{O}_5)\text{--}50\text{SrB}_4\text{O}_7$  samples.

**Figure 12.** The D.C. conductivity versus  $1000/T$  for  $x(2\text{Bi}_2\text{O}_3\text{--V}_2\text{O}_5)\text{--}(100\text{--}x)\text{SrB}_4\text{O}_7$  glasses.

**Figure 13.** The imaginary part versus real part of impedance (the Nyquist plot) for (a) SBO, (b) heat treated  $5(2\text{Bi}_2\text{O}_3\text{--V}_2\text{O}_5)\text{--}95\text{SrB}_4\text{O}_7$  and (c) fully crystallized  $50(2\text{Bi}_2\text{O}_3\text{--V}_2\text{O}_5)\text{--}50\text{SrB}_4\text{O}_7$  sample at 813K. The solid lines in the picture represent the results of fitting.

**Figure 14.** (a) The relaxation time and (b) conductivity with activation energy calculated with the use of Cole-Cole relation for SBO, heat treated  $5(2\text{Bi}_2\text{O}_3\text{--V}_2\text{O}_5)\text{--}95\text{SrB}_4\text{O}_7$  and fully crystallized  $50\text{SrB}_4\text{O}_7\text{--}50(2\text{Bi}_2\text{O}_3\text{--V}_2\text{O}_5)$  samples.

**Figure 15.** The  $\alpha$  parameter for SBO, heat treated  $5(2\text{Bi}_2\text{O}_3\text{--V}_2\text{O}_5)\text{--}95\text{SrB}_4\text{O}_7$  and fully crystallized  $50(2\text{Bi}_2\text{O}_3\text{--V}_2\text{O}_5)\text{--}50\text{SrB}_4\text{O}_7$  samples.

## Tables

**Table 1.** Glass transition, exothermic and endothermic processes temperatures for all as-quenched samples.



**Table 2.** The activation energy of conduction processes,  $\tau_0$ ,  $\sigma_0$  and  $A$  parameters for SBO, heat treated  $5(2\text{Bi}_2\text{O}_3\text{-V}_2\text{O}_5)\text{-95SrB}_4\text{O}_7$  and fully crystallized  $50(2\text{Bi}_2\text{O}_3\text{-V}_2\text{O}_5)\text{-50SrB}_4\text{O}_7$  samples at high temperature range.